Optimum Design of Artificial Lateral Line Systems for Object Tracking under Uncertain Conditions

Ali Ahrari
Department of mechanical engineering
Michigan State University,
East Lansing, MI, USA
ahrarial@msu.edu

Hong Lei
Department of electrical and computer engineering
Michigan State University,
East Lansing, MI, USA
leihongbuaa@gmail.com

Montassar Aidi Sharif
Department of electrical and computer engineering
Michigan State University,
East Lansing, MI, USA
engmas83@yahoo.com

Kalyanmoy Deb
Department of electrical and computer engineering
Michigan State University
East Lansing, MI, USA
kdeb@egr.msu.edu

Xiaobo Tan
Department of electrical and computer engineering
Michigan State University
East Lansing, MI, USA
xbtan@egr.msu.edu

Abstract An artificial lateral line (ALL) consists of a set of flow sensors arranged around a fish-like body, which can dynamically track an underwater moving object and estimate its parameters including size, shape, velocity and position by employing the extended Kalman filter (EKF); Nevertheless, the uncertainty in the sensors and in the employed flow model makes accurate tracking challenging. The goal of this study is to maximize the accuracy of tracking for an arbitrary object by proper selection of the design parameters including shape, size and the number and location of the sensors. It develops a robust parametric fitness function for quantifying the tracking accuracy. A comprehensive parameter study is rendered to find the set of parameters that minimizes the uncertainty in evaluation of a design. The magnitude of uncertainty in the model is estimated by performing a computational fluid dynamics simulation. Covariance matrix adaptation evolution strategy (CMA-ES) is then employed to determine optimum parameters of EKF and to optimize the ALL. Trade-off between the tracking accuracy and the number of sensors is also analyzed. Dependency of the optimum setting of the EKF and the design parameters on the amount of uncertainty in the problem is investigated as well.

Keywords: Extended Kalman filter; Object tracking; Sensor placement

1. INTRODUCTION

The lateral line system of fish is an important organ sensitive to fluid motion around the fish's body [1], and involved in various biological behaviors, such as schooling [2] station holding [3], and prey/predator detection [4]. A lateral line system comprises arrays of mechanoreceptive units called neuromasts, which function as flow sensors [5]. The superficial neuromasts, which stick out of the fish skin and respond to flow velocities, is one of the two types of neuromasts [6]. The interaction between the flow and the neuromasts generate neuronal pulses which are transmitted to the central nervous system for further information processing [7].

The biological lateral line has inspired a number of efforts in developing an engineering equivalent of analogous sensing modality for underwater applications. Such an artificial lateral line (ALL) system will function as a novel and noiseless sensing modality, and assist underwater robots and vehicles for the navigation and control when traditional underwater sensing strategies such as vision or sonar are inhibited [8, 9].

Some theoretical work has also been reported on flow modeling and information processing to extract information from ALLs [5, 10, 11]. While most of previous studies focused on the estimation of a vibrating source, called the dipole source [12, 13, 14], several other studies aimed at tracking moving objects or vortex [15, 16, 17, 18], where arrays of commercial pressure sensors are adopted. IPMC-based ALLs are also reported on tracking and estimating a moving cylindrical object by measuring the flow velocities, analogous to the superficial neuromasts, and applying the Kalman filter strategy [18].

Although studies have been conducted on the tracking and estimation of moving objects using the ALL system, very few has addressed the identification of an optimal ALL, the one that provides maximum estimation accuracy for an arbitrary moving object. In a previous study [11], the placement of flow sensors was optimized based on observability for the control purpose. The proposed estimation and optimization were performed in a uniform flow field, different from the tracking of a moving object. Moreover, the adopted flow model was commonly assumed to be accurate while like most other theoretically driven models, it relies on assumptions that may not meet practical situations.

Unlike most previous studies on ALLs, this article develops an evolutionary bi-objective design tool for an ALL, including the shape, size, and the number of locations of flow velocity sensors,

such that the accuracy of tracking is maximized for an arbitrary moving object. In particular, an ALL is used to dynamically track a moving cylindrical object and estimate its parameters including size, shape, velocity, and position by applying the extended Kalman filter (EKF) strategy. This dynamic tracking problem is fundamentally different from identification of a vibrating dipole. The uncertainty in the sensors and in the employed flow model is simulated in this study, making it challenging to accurately track the moving object. Therefore, a robust parametric fitness function is first developed to quantify the tracking accuracy. A comprehensive parameter study is then rendered to find the set of parameters that minimizes the uncertainty in evaluation of a design. The magnitude of uncertainty in the model is estimated by comparing results of the computational fluid dynamics (CFD) simulation and available theoretical results. The study is interesting from (1) handling of noise in evaluation function, (2) inverse problem solving, and (3) a bi-objective optimal design of an artificial lateral line system for tracking underwater moving objects.

The rest of this paper is organized as follows. In Section 2, the tracking problem is formulated and extended Kalman Filter is employed to solve the tracking problem. In Section 3, the optimization problem is discussed and a parametric fitness function is proposed. Parameter study is performed in Section 4 and optimization results are provided in Section 5. Finally, conclusions are drawn in Section 7.

2. PROBLEM FORMULATION

The goal of the ALL system is to identify parameters of a moving object with ellipsoidal profile and to track its position using an array of flow sensors, as illustrated in Figure 1. The ALL consists of a number of sensors, located in xy plane, with the sensor locations denoted as (x_i, y_i), $1 \leq i \leq N_{sensor}$. For ease of buildability, the sensors are mounted perpendicular to the ALL body, therefore, the sensing direction would be parallel to the body at the place of the sensors. Each sensor provides a noisy measurement of the local flow velocity along its sensing direction, denoted by $M_i(t)$. $[x_s(t), y_s(t)]$ specifies the position of the center of the moving cylindrical shape at time t. The object is assumed to move at a constant speed of v_x along the x coordinate. This motion causes a disturbance and a flow field around the object which can be computed using a potential flow model:

$$M_i(t) = f(\boldsymbol{\theta}(t), [x_i, y_i]) \tag{1}$$

where $M_i(t)$ is the local flow velocity at the place of sensor i and $\boldsymbol{\theta}(t)$ represents parameters of the moving object. Function f is derived by the employed flow model. Having the local flow velocity at the place of sensors ($\boldsymbol{M}(t)=M_1(t)$, $M_1(t)$, …, $M_{Nsensor}(t)$), $\boldsymbol{\theta}(t)$ can be determined, e.g. the moving object can be reliably tracked; however, due to presence of noise in the sensor measurements and uncertainty in the employed flow model, there is always a tracking error. The tracking error for an arbitrary moving object can be minimized by proper section of the ALL parameters, including, the shape, size, number and location of sensors on the body, which is the goal of this study.
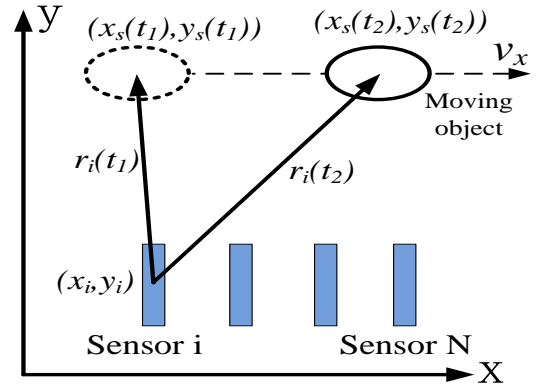

Figure 1. Illustration of the tracking of a moving object

2.1. Potential flow model

Consider a cylindrical object moving through still fluid, where the boundary effect can be ignored. Initially the object is assumed to be a cylinder with spherical cross-section. Later, the model is generalized to an arbitrary cross-section profile using the conformal mapping theory. It is also assumed that the cylinder is moving along the x–direction while its axis remains aligned with the z-axis. The cylindrical object has infinite length, therefore, the flow field is two-dimensional (2D) within the x–y plane. The potential flow theory is used to describe this flow field. The complex potential $w^c(z)$, where $z = x+iy$ is outside the region occupied by the cylinder, is given by [19]:

$$w^c(z) = v_x \frac{R^2}{z - z_1}, \tag{2}$$

where the superscript c denotes that the cross section is circular. v_x is the constant moving speed, R is a radius of the circular cross-section, and $z_1 = x_s+iy_s$ represents the center of the moving cylinder. The corresponding complex flow velocity W^c is computed as follows:

$$W^c(z) = \frac{dw^c(z)}{dz} = -v_x \frac{R^2}{(z - z_1)^2}. \tag{3}$$

For $W^c(z) = v_x^c + iv_y^c$, the local velocity field can be determined as follows:

$$v_x^c = \frac{v_x R^2 ((x - x_s)^2 - (y - y_s)^2)}{((x - x_s)^2 + (y - y_s)^2)^2}, \tag{4}$$

$$v_y^c = \frac{2v_x R^2 (y - y_s)(x - x_s)}{((x - x_s)^2 + (y - y_s)^2)^2}. \tag{5}$$

For a cylinder with an arbitrary cross-section profile, the shape of the cross-section can be obtained by mapping the circular profile with the Laurent series expansion [20]:

$$\zeta(z) = (z - z_1) + \frac{\lambda_1}{(z - z_1)} + \frac{\lambda_2}{(z - z_1)^2} + \cdots \tag{6}$$

where λ_1, λ_2, …, defines the shape. The resultant shape would be symmetric about the x–direction if the shape parameters are real. For such a general profile, the complex flow velocity $W^g(z)$ around the moving object is calculated as follows:

$$W^g(z) = \frac{dw^c(z)}{dz}\frac{dz}{d\zeta}$$
$$= \underbrace{v_x\left(-\frac{R^2}{(z-z_1)^2}\right)}_{W^c(z)}\underbrace{\left(1 - \frac{\lambda_1}{(z-z_1)^2} - \cdots\right)^{-1}}_{\frac{dz}{d\zeta}}, \qquad (7)$$

where z is an arbitrary point outside the cylindrical object. We limit our discussion to the case of ellipsoidal profile, where only $\lambda_1 \geq 0$ is nonzero. It is notable that the effect of higher-order terms in this equation decays quickly when the distance from the object increases. The complex flow velocity $W^e(z)$ around an ellipsoidal cylinder is computed as follows:

$$W^e(z) = v_x\left(-\frac{R^2}{(z-z_1)^2}\right)\left(1 - \frac{\lambda_1}{(z-z_1)^2}\right)^{-1} \qquad (8)$$

For $W^e(z) = v_x^e + iv_y^e$, it results in:

$$v_x^e = \frac{v_x R^2((x-x_s)^2 - (y-y_s)^2 - \lambda_1)}{((x-x_s)^2 + (y-y_s)^2 - \lambda_1)^2 + 4(x-x_s)^2(y-y_s)^2}, \qquad (9)$$

$$v_y^e = \frac{2v_x R^2(y-y_s)(x-x_s)}{((x-x_s)^2 + (y-y_s)^2 - \lambda_1)^2 + 4(x-x_s)^2(y-y_s)^2}. \qquad (10)$$

These equations are employed to compute the local flow around the moving cylinder.

2.2. Extended Kalman Filter

Kalman filter is one of the most popular and robust techniques for estimation of system states subject to measurement and model uncertainties. The extended Kalman filter (EKF) is employed in this study to track the object because of the nonlinearities in the system behavior.

At the k-th time step, the EKF predicts the state as follows:

$$\boldsymbol{\theta}_k = \mathbf{A}_k \boldsymbol{\theta}_{k-1} \qquad (11)$$

where

$$\mathbf{A}_k = \begin{bmatrix} 1 & 0 & 0 & \Delta t & 0 \\ 0 & 1 & 0 & 0 & 0 \\ 0 & 0 & 1 & 0 & 0 \\ 0 & 0 & 0 & 1 & 0 \\ 0 & 0 & 0 & 0 & 1 \end{bmatrix}, \boldsymbol{\theta}_k = \begin{bmatrix} x_s \\ y_s \\ \lambda_1 \\ v_x \\ R^2 \end{bmatrix}$$

specify the system behavior and state at the k-th time step, respectively. The predicted estimate covariance is computed as follows:

$$\boldsymbol{P}_k = \mathbf{A}_k \boldsymbol{P}_{k-1} \mathbf{A}_k^{-1} + \mathbf{Q}_k \qquad (12)$$

where $\mathbf{Q}_k$ is the process noise covariance. The optimum Kalman gain is computed then:

$$\boldsymbol{K}_k = \boldsymbol{P}_k \mathbf{H}_k^T\left(\mathbf{H}_k \boldsymbol{P}_k \mathbf{H}_k^T + \mathbf{C}_k\right)^{-1}, \qquad \mathbf{H}_k = \left.\frac{\partial f(\boldsymbol{\theta})}{\partial\boldsymbol{\theta}}\right|_{\boldsymbol{\theta}=\boldsymbol{\theta}_k} \qquad (13)$$

which is used to update the previous estimate on the k-th state:

$$\boldsymbol{\theta}_k \leftarrow \boldsymbol{\theta}_k + \boldsymbol{K}_k\left(\mathbf{M}_k - f(\boldsymbol{\theta}_k)\right) \qquad (14)$$

Finally, the predicted estimate covariance is updated:
$$\mathbf{P}_k \leftarrow (\mathbf{I} - \mathbf{K}_k \mathbf{H}_k)\mathbf{P}_k \qquad (15)$$

For the time step $k+1$, this process repeats from equation 11.

2.3. Simulation of Uncertainties
The employed flow model assumes some ideal conditions, which to some extent, are not available in practice. For example, the

sensor and the ALL body affect the flow field; therefore, the actual local flow velocity is different from the one computed using the flow model. At the same time, sensor measurement at the k-th time step (M_k) can be slightly different from the true local velocity ($\underline{M}_k$) due to limited precision of the sensors. These uncertainties are simulated into the problem as follows: First, a proportional noise is applied to the flow model to simulate the uncertainty of the flow model:

$$\underline{M}_k = f(\underline{\boldsymbol{\theta}}_k) \times \exp(\varepsilon_{\text{model}}N(0,1)), k = 1,2,\dots,N_{\text{sample}} \qquad (16)$$

where $\varepsilon_{\text{model}}$ specifics standard deviation of the relative error of the flow model. An additive noise is applied to this value to simulate the noisy sensor measurements:

$$M_k = \underline{M}_k + \varepsilon_{\text{sensor}}N(0,1), \quad k = 1,2,\dots,N_{\text{sample}} \qquad (17)$$

where $\varepsilon_{\text{sensor}}$ is the standard deviation of the sensor measurement error. Following the experiment in [13], $\varepsilon_{\text{sensor}}=0.0015$ cm/s is assumed.

2.4. Object Tracking Using EKF
EKF employs an iterative process for which the initial estimate ($\underline{\boldsymbol{\theta}}_0$) and the initial values of matrices $\mathbf{C}$, $\mathbf{P}$ and $\mathbf{Q}$ should be provided. For our problem, the initial estimate is generated inside a cube of side length of c_{ini}, centered on $\underline{\boldsymbol{\theta}}_0$:

$$\boldsymbol{\theta}_0 = \underline{\boldsymbol{\theta}}_0 + c_{\text{ini}}(\boldsymbol{U}_5(0,1) - \mathbf{0.5}), \qquad (18)$$

where $\boldsymbol{U}_5(0,1)$ is a vector of five random numbers sampled from the standard uniform distribution. The initial values of $\mathbf{P}$ (estimate error covariance), $\mathbf{Q}$ (process noise covariance) and $\mathbf{C}$ (measurement noise covariance) are $p_0\mathbf{I}$, $q_0\mathbf{I}$ and $c_0\mathbf{I}$ respectively and are set as follows:

- p_0 depends on the value of c_{ini}. Since variance of the standard uniform distribution is 1/12, we set $p_0=(c_{\text{ini}})^2/12$.

- c_0 is set to be the variance of sensor uncertainty ($\varepsilon_{\text{sensor}}^2$).

- q_0 encompasses the effect of model noise. The model noise is almost equal to $\varepsilon_{\text{model}}M$, which depends on the location of the cylinder. For simplicity, we estimated the average local speed by Monte Carlo simulation ($M_{\text{ave}}\approx 0.25$ cm/s) and then set $q_0 = \varepsilon_{\text{model}}M_{\text{ave}}$.

These a priori set values are used for analysis of the problem. In Section 4.1, the optimum values of these parameters are derived and compared with a priori values.

The object moves all the way from the left to right, inside a rectangle above the ALL. The range of parameters of the cylinder are set as follows: 2 cm/s $\leq v_x \leq$ 10 cm/s; 0 cm$^2 \leq \lambda_1 \leq$ 9 cm^2;1 cm$^2 \leq R^2 \leq$ 9 cm^2.

For each state, the EKF is utilized to update the estimate of the parameters of the object. The tracking process starts from $\underline{x}_s= -10$ cm and continues to $\underline{x}_s= +10$ cm. The time interval of sampling is 0.01 second. Depending on the velocity of the object, the number of sampled signals (N_{sample}) may vary from 200 to 1000. We also set $c_{\text{ini}}=5$.

Figure 2 illustrates the tracking results for a sample object with $\underline{\boldsymbol{\theta}}_0=[-10, 7, 1, 9, 5]$. The EKF provides the estimate $\boldsymbol{\theta}_k$ which after some steps may converge to the actual object parameters. For a given M_k, the tracking error is then defined as follows:

$$e_k = \left\| \left[\frac{\underline{x}_s - x_s}{1 \text{ cm}}, \frac{\underline{y}_s - y_s}{1 \text{ cm}}, \frac{\underline{\lambda}_1 - \lambda_1}{1 \text{ cm}^2}, \frac{\underline{v}_s - v_s}{1 \frac{\text{cm}}{\text{s}}}, \frac{\underline{R}_s^2 - R_s^2}{1 \text{ cm}^2} \right] \right\|_k \quad (19)$$

where the underlined parameters refer to the actual object. This equation defines that the tracking error at state k as the Euclidean norm of $\underline{\theta}_k - \theta_k$, which is made dimensionless to avoid dimension mismatch when calculating the norm. The tracking error is computed for each of these states, resulting in the vector of errors e. Algorithm 1 explains the tracking process and computation of e while uncertainties are encompassed in the simulation.

Algorithm 1. Tracking and calculation of tracking error

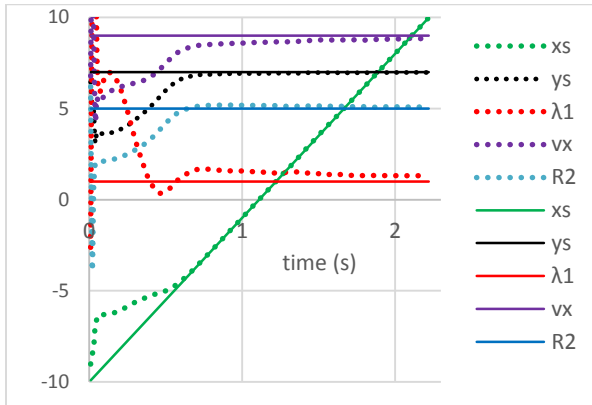|	
	Input: Initial state of the object
	Output: tracking error e
L1:	Initialize the parameters of the EKF
L2:	generate the initial estimate (θ) randomly
L3:	for k=1 to N_{sample}
L4:	Simulate M_k using equations 16 and 17
L5:	Update θ_k using the EKF and M_k
L6:	Compute e_k using equation 19
L7:	$\theta_1 \leftarrow \theta_4 + \theta_1 \Delta t$
L8:	$\underline{\theta}_1 \leftarrow \underline{\theta}_4 + \underline{\theta}_1 \Delta t$
L9:	End

Figure 2. Tracking of a sample object a) Sample and the ALL and b) tracking estimate (dots) and the true values (continuous lines) for a typical cylindrical object

3. OPTIMIZATION PROBLEM

The ultimate goal of the ALL design optimization problem is to find the optimal shape and size of the body and the locations of sensors on its body such that for a given number of sensors, the tracking accuracy is maximized. In this section, the design optimization problem is formulated and the design parameters, their ranges, constraints, the fitness function, and the optimization method to solve the problem are explained.

3.1. Fitness Function

It should be noted that in general, the cylinder may move anywhere in the predefined working area. Since considering all possible cases is not possible, the tracking problem is solved for a finite number (N_{cyl}) of cylinders. A simple fitness function can be defined as the mean of all tracking errors; however, the mean is not a robust statistic. The mean is highly affected by possible outliers. Considering different sources of uncertainties, a robust performance measure is strongly desired. The proposed fitness function follows this goal. First, a score for tracking accuracy in case of a single moving cylinder is defined:

$$g(X, \theta) = \sum_{k=1}^{N_{\text{sample}}} w_k \exp(-\zeta e_k^2), \quad (20)$$

which gives a tracking credit based on the tracking accuracy. w_i is the weight for each estimation:

$$w_k = \frac{2k}{N_{\text{sample}} \times (N_{\text{sample}} + 1)}$$

more credit is allocated for final estimations. Parameter ζ determines how fast the obtained credit reduces when the estimation error increases. The calculated credit increases if ζ is reduced. Selection of an appropriate value for this parameter is discussed in Section 4.3. The fitness of a design is then computed by averaging the credits gained for tracking of N_{cyl} objects:

$$g(X) = \frac{1}{N_{\text{cyl}}} \times \sum_{j=1}^{N_{\text{cyl}}} g(X, \theta_j) \quad (21)$$

It is notable that because of sensor and flow model uncertainties, random selection of a finite number of moving objects, and random initial estimate of the EKF, there is *uncertainty* in evaluation of the fitness, a matter which is common in robust optimization studies [21, 22]. The fitness function $g(X)$ is a random function, therefore, mean and standard deviation ($\bar{g}$, s_g) can be computed over multiple independent evaluation of a single design. This uncertainty in fitness evaluation results in selection noise, which adversely affects reliability of the selection operator and as a consequence, the quality of the optimized solution.

3.2. Design Parameters and Constraints

The conformal mapping technique is employed to define the cross-section profile of the cylindrical body and the location of sensors on it. For the complex plan $\mathbb{C}$ and a point $\xi \in \mathbb{C}$, ξ is mapped to z with respect to the transformation variable $\lambda \in \mathbb{R}$ using the following transformation [19]:

$$z = \xi + b^2/\xi, \xi = R \exp(i\beta) - \lambda, b = R - \lambda, \beta \in [-\pi, \pi). \quad (22)$$

This equation defines a disk of radius R, offset along the real axis by $\lambda \in \mathbb{R}$. By choosing b, we can map the disk to a symmetric, streamlined body (Figure 3). Therefore, R and λ specify the size and the shape of the body, and β_k denotes location of the k-th sensor on the fish body. The ALL body turns to a circle and a line segment for $\lambda/R = 1$ and $\lambda/R = 0$, respectively. Other values between these two extremes result in a fish-like ALL.
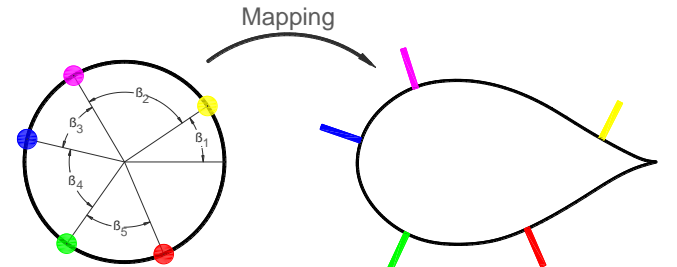

Figure 3 conformal mapping from a sphere to a streamline body

Because of symmetry, only the locations of the sensors on the upper side of the ALL are independent. Moreover, the object may move above the ALL; therefore, the lower part of the ALL is ignored. The set of design variables, $X=[X_1, X_2, …, X_D]$ consists of:

- Size variable: $X_{1\min} \leq X_1 = R \leq X_{1\max}$

- Shape variable: $X_{2min} \leq X_2 = \lambda/R \leq X_{2max}$.
- Angular position of the first sensor on the fish body: $0 \leq X_3 = \beta_1 \leq \beta_{max}$.
- Angular position of the k-th sensor relative to the $(k-1)$-th sensor: $0 \leq X_k = \beta_{k-2} - \beta_{k-1} \leq \beta_{max}$, $k = 4, 5, \ldots, N_{sensor}$.

where N_{sensor} specifies the number of sensors in the upper part of the ALL. A constrain is defined so that all the active sensors lie on the upper part of the ALL:

- $X_3 + X_4 + \ldots + X_{N_{sensor}} \leq \pi$

For the rest of this study, the following values for the range of design parameters are considered, unless mentioned otherwise: $X_{1min} = 0.5$ cm, $X_{1max} = 4$ cm, $X_{2min} = 0$, $X_{2max} = 1$, $\beta_{max} = 4\pi/N_{sensor}$. Furthermore, for ease of construction, the sensing direction of a sensor is assumed to be tangent to the body at the place of the sensor.

3.3. Optimization Method

We employ covariance matrix adaptation evolution strategy (CMA-ES) [23] for optimization of these parameters. CMA-ES belongs to the category of evolution strategies that adapt the full covariance matrix. It was ranked first in BBOB2009 completion on noisy continuous parameter optimization [24]. CMA-ES is therefore a suitable choice for our noisy problem where for a fixed N_{sensor}, all parameters are continuous.

All the parameters of CMA-ES are set to the default values, as explained in [25], except the population size. For the problem at hand, we start from a large population size S_{max}, but a small value of N_{cyl}, and gradually reduce the population size and increase N_{cyl}. The reason is that a larger population size enables a better global exploration in the early iterations; however, since N_{cyl} is small, the noise is great and the population cannot converge to the exact location of the optimum. To alleviate this problem, N_{cyl} is gradually increased and the population size is reduced so that the computation per iteration does not change much.

4. PARAMETER STUDY

To optimize the ALL, N_{cyl}, ζ, and ε_{model} should be specified. By proper selection of these parameters, we can minimize the selection noise or reach a higher tracking accuracy. Selection noise can be reduced if the variance among the true fitness of designs is maximized or when the variance of the estimated fitness under independent evaluations is minimized [13]. Accordingly, Selection Reliability Index (SRI) can be defined as follows:

$$SRI = \frac{StDev(\bar{g})}{mean(s_g)}. \tag{23}$$

A larger SRI usually refers to a smaller selection noise. A parameter study is performed in this section to monitor the effect of different parameters on SRI, which helps select a reasonable parameter setting. To study the effect of different parameters, 250 random designs $(X_1, X_2, \ldots, X_{250})$ are generated with $N_{sensor} = 4, 6, 8, 10, 12$ (50 of each). Since there are many parameters, we study a few at a time while the rest are set to some default values unless mentioned otherwise. The default values are as follows: $N_{cyl} = 200$, $\zeta = 1$ and $\varepsilon_{sensor} = 0.0015$ cm/s, while different values of ε_{model} are considered. Parameters of the EKF are set to a priori values.

4.1. EKF Parameters

For a fixed value of ε_{model} and N_{sensor}, we optimize parameters of the EKF ($z = [c_0, p_0, q_0]$) such that average fitness of 50 random designs (with identical number of sensors) is maximized. This procedure is performed for $\varepsilon_{model} = 0.01, 0.05, 0.2$ and $N_{sensor} = 4, 6, 8, 10, 12$, and thus 15 vectors of $z^*(\varepsilon_{model}, N_{sensor})$ are found.

For optimization, we employ CMA-ES, as discussed in Section 3.3. The maximum number of iterations is set to 100 while N_{cyl} increases from 10 to 50 and the population size reduces from 50 to 10. An exponential transformation of the search space ($z = \exp(z')$) is employed so that z always remains positive and unconstrained optimization performs in the z' space.

Figure 4a illustrates average fitness of 50 designs with different number of sensors, when $z^*(0.05, 4), z^*(0.05, 6), \ldots, z^*(0.05, 12)$ are applied as the initial values of the EKF. It demonstrates that z^* is independent of N_{sensor} and thus if z^* is optimized for $N_{sensor} = 4$, it can be applied to the problem with $N_{sensor} = 12$ with no reduction in fitness. It can also be observed that random designs with more number of sensors have a higher fitness on average.

Figure 4b illustrates that $z^*(0.05, N_{sensor})$ are not similar; however, there is a relation between them: for any two z^*, the ratio of $[c_0, p_0, q_0]$ is similar. This means only two of these values are independent, and multiplication of a given set of initial values by a fixed positive number does not change the average fitness.

Figure 4c illustrates average fitness of 50 designs in situations with different values of ε_{model}, when $z^*(0.01, 8), z^*(0.05, 8)$, and $z^*(0.20, 8)$ are applied as the initial values of the EKF. Unlike the previous case, some dependency of z^* on ε_{model} is observable. More importantly, there is significant fitness decline if a priori set values are applied as initial condition of the EKF. This demonstrates the importance of setting the EKF parameters to their optimal values.
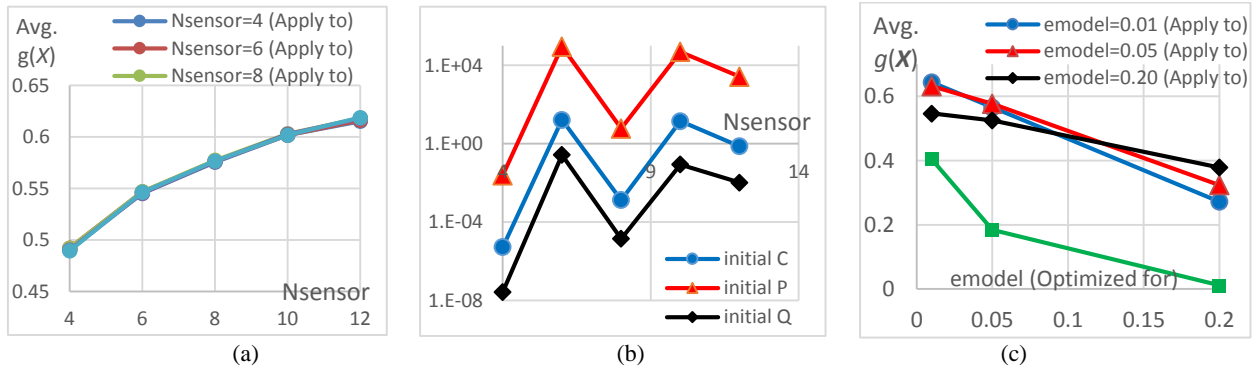

Figure 4. a) Average fitness of 50 designs evaluated when $\varepsilon_{model} = 0.05$, and $z^*(0.05, N_{sensor})$ is applied. b) $z^*(0.05, N_{sensor})$ for $\varepsilon_{model} = 0.05$. c) Average fitness of 50 designs when $N_{sensor} = 8$, and $z^*(\varepsilon_{model}, 8)$ is applied as the initial values of the EKF.

4.2. Effect of N_{cyl}

More sample objects provide a more accurate representation of all possible objects in the considered range. It also moderates the effect of randomness caused by random initial estimates as well as random simulated amount of model and sensor errors. The result is a better evaluation of the design or equivalently, a smaller s_g. This benefit comes at the cost of proportional growth of computation time. Figure 5 depicts mean (s_g) and SRI for the 250 random designs, when evaluated 20 times independently. It demonstrates that:

- A sufficiently great SRI can be reached provided that N_{cyl} is is sufficiently great. This means the disruptive effect of evaluation noise can be subsided as much as desired by increasing N_{cyl}. The effect is almost independent of the value of ε_{model}.

- Mean (s_g) demonstrates the limit for accuracy of final results. Since the evaluation uncertainty can result in overestimation of the fitness up to $2s_g$, the true fitness of the found global minimum value might be $2s_g$ less than the one computed by the algorithm. Similarly, sufficiently small values of s_g can be reached by higher values of N_{cyl}.
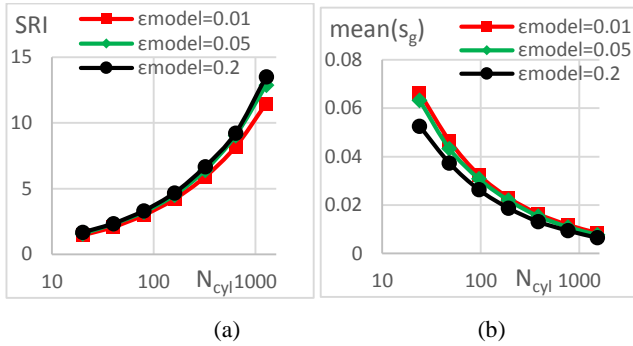

(a) (b)

Figure 5. Effect of N_{cyl} and ε_{model} on SRI and mean(s_g)

4.3. Effect of ζ

The fitness function requires parameter ζ to be set. As it was discussed in Section 3.1, a lower ζ returns a higher fitness value. The importance of this parameter attributes to its effect on SRI. A too small value results in a high fitness (close to one) for all solutions, which reduces the variance of the true fitness of different designs, and consequently reduces SRI. Similarly, a too large value leads to a low fitness (close to zero) for all solutions, which lowers SRI as well. In this section, the 250 random designs are evaluated for different values of ζ ($N_{cyl}=200$). SRI and the average fitness are plotted in Figure 6, which demonstrates that $\zeta \geq 1$ is a proper choice considering SRI, although the optimal value depends ε_{model} as well. For the rest of this study, we set $\zeta=1$.
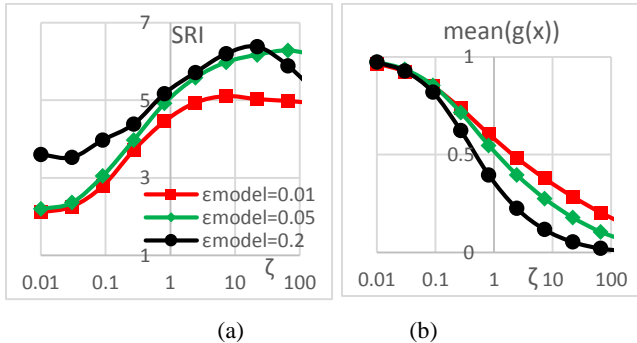

(a) (b)

Figure 6. Effect of ζ on a) SRI and b) average fitness for different values of ε_{model}.

4.4. Estimation of ε_{model}

In this section, the value of ε_{model} is estimated by performing a computational fluid dynamics (CFD) simulation and comparing the results with those of the employed flow model. A cylinder with circular cross-section is moving along the x-axis. The cylinder has a diameter of 0.85cm, and velocity of 6cm/s. The motion starts at [–40 cm, 0 cm] at time t=0. To reduce the effect of boundaries, a larger tank is considered which spans 120cm in length, 120cm in width, and 50cm in depth. The time duration for the translating is 15 seconds. The CFD simulation was rendered in FLOW-3D® which solves Navier-Stokes equations.
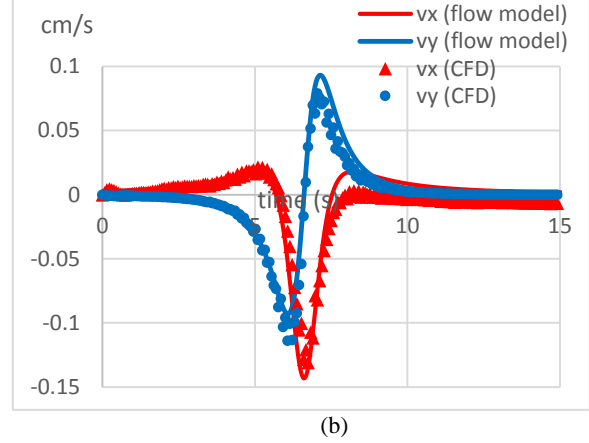

(b)

Figure 7. CFD simulation a) setup b) CFD and flow model results.

Figure 7 shows the CFD and the potential flow model velocity components at the sensors place. As it can be observed, there is a reasonable agreement between the flow model and CDF results. In addition to limited size of the tank in the CFD model, consideration of viscosity can also justify the difference between the CDF and flow model results to some extent. A relative difference of 38% was found between the flow model and CFD prediction. If it is assumed that the CFD simulation represents the reality, ε_{model} can be computed as follows:

$$E[\varepsilon_{model}|\mathcal{N}(0,1)] = \frac{\sum_k^{100}\left(\left|v_x^e - v_x^{CFD}\right|_k + \left|v_y^e - v_y^{CFD}\right|_k\right)}{\sum_k^{100}\left(\left|v_x^{CFD}\right|_k + \left|v_y^{CFD}\right|_k\right)}. \quad (24)$$

Using this equation and the CFD simulation results concludes to $\varepsilon_{model}=0.48$, which is rather high value.

5. OPTIMIZATION RESULTS

We consider two cases with different amount of model uncertainty ($\varepsilon_{model}=0.01$, 0.20). The ALL is optimized using CMA-ES given the optimum parameters of the EKF. The trade-off between the number of sensors and the accuracy of tacking is investigated by running CMA-ES for different values of N_{sesnor} independently. The population size reduces from 150 to 30 while N_{cyl} increases from 200 to 1000. The evaluation budget is limited to 3×10^6 sample objects.

For each value of ε_{model} and N_{sensor}, CMA-ES is run five times independently. Figure 8 depicts the final solutions for $\varepsilon_{model}=0.01$ and 0.20 for the case $N_{sensor}=6$. The average values of size parameter (R) and shape (λ/R) are plotted as a function of N_{sensor} in Figure 9. To check dependency of the final solutions on the ε_{model}, the final solutions for $\varepsilon_{model}=0.01$ and $\varepsilon_{model}=0.20$ are reevaluated in both conditions of $\varepsilon_{model}=0.01$ an $\varepsilon_{model}=0.20$ with a large number of sample objects ($N_{cyl}=10000$). The reevaluated fitness is plotted in Figure 10. The obtained results reveal:
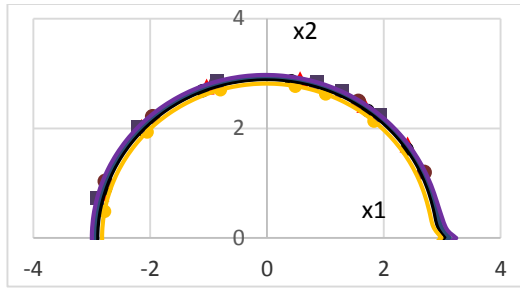
(a)
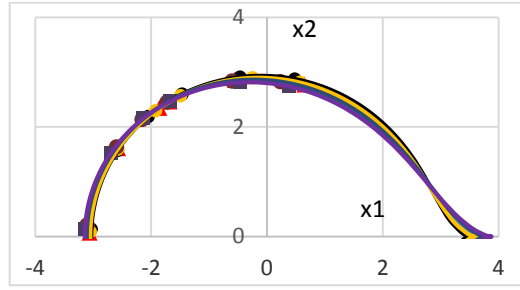
(b)

Figure 8. Final solution for N_{sensor}=6 when a) ε_{model}=0.01 and b) ε_{model}=0.20

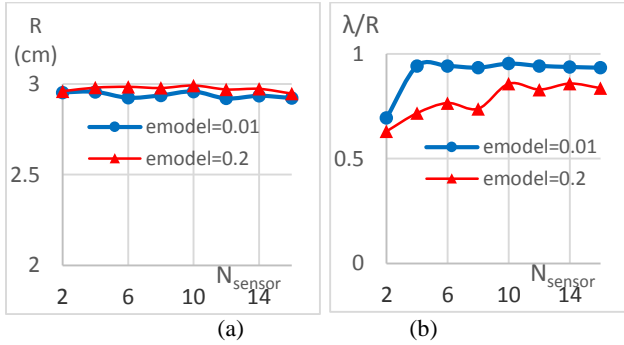(a)   (b)

Figure 9. Average values of the size (R) and shape (λ/R) parameters in the final designs

(a)   (b)
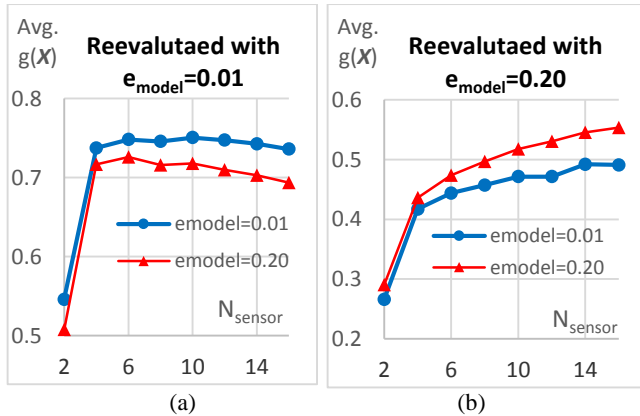
Figure 10. Average fitness of the optimized designs for ε_{model}=0.01 and ε_{model}=0.20 reevaluated in the condition of ε_{model}=0.01 and ε_{model}=0.20

- For a fixed amount of uncertainty, the final solutions of independent runs are similar (Figure 8). This can be regarded as a checkpoint for efficacy of the optimization tool.

- The shape parameter is smaller for ε_{model}=0.20 (Figure 9). For both cases, the size parameter (R) has reached the upper bound A larger design enables measuring local velocity at different regions and therefore improves the diversity of the information gathered by the sensors; however, it occupies a larger region. Assuming the objects cannot move through the ALL, a larger design limits the situations in which an object can be tracked.

- For the case with low uncertainty, increasing the number of sensors is advantageous up to N_{sensor}=4 (Figure 10). After that, the extra sensors do not provide any contribution for tracking. In fact, the fitness of the optimized designs declines for $N_{sensor}\geq12$. One reason for this observation can be the complexity in the problems with more number of sensors, e.g. more design parameters, which demands a more computation budget. The evaluation budget of CMA-ES was independent of the number of design parameters; therefore, the algorithm could not properly explore the search space for $N_{sensor}\geq12$.

- For the case with high amount of uncertainty, increasing N_{sensor} continually improves the tracking accuracy. This means the contribution of extra sensors is significant in comparison with the increased problem complexity.

- The ALL optimized for ε_{model}=0.01 is not the optimal one for ε_{model}=0.20 (Figure 10). This means the optimal design depends on the mount of uncertainty.

6. SUMMARY AND CONCLUSIONS

In this study, design of artificial lateral line system was optimized for maximizing tracking accuracy for an arbitrary moving object by using extend Kalman filter. The parameters of the filter were optimized as well. Trade-off between the number of sensors and the tracking accuracy was also analyzed for different amount of uncertainties.

It was demonstrated that for this problem, the optimal setting of parameters of the extended Kalman filter plays a significant role in reliability of tracking. A priori set values turned out to be far from the optimal ones, determined by performing parameter optimization. Our numerical results revealed dependency of the optimum design as well as the filter parameters on the amount of uncertainty. The obtained trade-off between the number of sensors and tracking accuracy can provide useful information to determine the number of sensors in the design. For our problem, the trade-off demonstrated that the contribution of extra sensors can be significant when the uncertainty is high, while it is negligible when the uncertainty is small.

7. ACKNOWLEDGEMENT

References

[1] H. Bleckmann, Reception of hydrodynamic stimuli in aquatic and semiaquatic animals, Stuttgart: Gustav Fischer Verlag, 1994.

[2] T. J. Pitcher, B. L. Partridge and C. S. Wardle, "A blind fish can school," *Science,* vol. 194, pp. 963-965, 1976.

[3] H. Bleckmann, A. Przybilla, A. Klein, A. Schmitz, S. Kunze and C. Brücker, "Station holding of trout: behavior, physiology and hydrodynamics.," in *Nature-inspired Fluid Mechanics*, Berlin Heidelberg, Springer, 2012, pp. 161-177.

[4] C. Von Campenhausen, I. Riess and R. Weissert, "Detection of stationary objects by the blind cave fish anoptichthys jordani (Characidae)," *Journal of comparative physiology,* vol. 143, no. 3, p. 369–374, 1981.

[5] E. S. Hassan, "Mathematical description of the stimuli to the lateral line system of fish derived from a three-dimensional flow field analysis," *Biological Cybernetics,* vol. 66, no. 5, pp. 443-452, 1993.

[6] J. Engelmann, W. Hanke, J. Mogdans and H. Bleckmann, "Hydrodynamic stimuli and the fish lateral line," *Nature,* vol. 408, no. 6808, pp. 51-52, 2000.

[7] H. Bleckmann, "Peripheral and central processing of lateral line information," *Journal of Comparative Physiology A,* vol. 194, no. 2, pp. 145-158, 2008.

[8] L. DeVries, F. Lagor, H. Lei, X. Tan and D. Paley, "Distributed flow estimation and closed-Loop control of an underwater vehicle with a multi-modal artificial lateral line," *Bioinspiration & Biomimetics,* vol. 10, no. 2, p. 025002, 2015.

[9] H. Lei, W. Li and X. Tan, "Microfabrication of IPMC cilia for bio-inspired flow sensing," in *Proc. of SPIE 8440, Electroactive Polymer Actuators and Devices (EAPAD)*, San Diego, California, 2012.

[10] Z. Ren and K. Mohseni, "A model of the lateral line of fish for vortex sensing," *Bioinspiration & Biomimetics,* vol. 7, no. 3, p. 036016, 2012.

[11] L. DeVries and D. A. Paley, "Observability-based optimization for flow sensing and control of an underwater vehicle in a uniform flowfield," in *Proc. of American Control Conf.*, Washington, DC, 2013.

[12] A. T. Abdulsadda and X. Tan, "Nonlinear estimation-based dipole source localization for artificial lateral line systems," *Bioinspiration & biomimetics,* vol. 8, no. 2, p. 026005, 2013.

[13] A. Ahrari, H. Lei, M. A. Sharif, K. Deb and X. Tan, "Design optimization of artificial lateral Line system under uncertain conditions," in *Proc. of IEEE congress on Evolutionary Computation (CEC 2015)*, Sendai, Japan, (to appear), 2015.

[14] A. M. K. Dagamseh, T. S. J. Lammerink, M. L. Kolster, C. M. Bruinink, R. J. Wiegerink and G. J. M. Krijnen, "Dipole-source localization using biomimetic flow-sensor arrays positioned as lateral-line system," *Sensors and Actuators A,* vol. 162, no. 2, p. 355–360, 2010.

[15] L. D. Chambers, O. Akanyeti, R. Venturelli, J. Ježov, J. Brown, M. Kruusmaa, et and al., "A fish perspective: detecting flow features while moving using an artificial lateral line in steady and unsteady flow," *Journal of The Royal Society Interface,* vol. 11, no. 99, p. 20140467, 2014.

[16] A. T. Abdulsadda and X. Tan, "Underwater tracking of a moving dipole source using an artificial lateral line: algorithm and experimental validation with ionic polymer–metal composite flow sensors," *Smart Materials and Structures,* vol. 22, no. 4, p. 045010, 2013.

[17] R. Venturelli, O. Akanyeti, F. Visentin, J. Ježov, L. D. Chambers, G. Toming, et and al., "Hydrodynamic pressure sensing with an artificial lateral line in steady and unsteady flows," *Bioinspiration & biomimetics,* vol. 7, no. 3, p. 036004, 2012.

[18] A. T. Abdulsadda and X. Tan, "Underwater Tracking and Size-Estimation of a Moving Object Using an IPMC Artificial Lateral Line," in *Proc. of ASME 2012 Conference on Smart Materials, Adaptive Structures and Intelligent Systems*, 2012.

[19] R. L. Panton, Incompressible Flow, John Wiley and Sons, 1984.

[20] R. Bouffanais, G. D. Weymouth and D. K. Yue, "Hydrodynamic object recognition using pressure sensing.," in *Proc. of Royal Society of London A: Mathematical, Physical and Engineering Sciences*, 2010.

[21] H. G. Beyer and B. Sendhoff, "Robust optimization–a comprehensive survey," *Computer Methods in Applied Mechanics and Engineering,* vol. 196, no. 33, pp. 3190-3218, 2007.

[22] J. S. Kang, T. Y. Lee and D. Y. Lee, "Robust optimization for engineering design. Engineering Optimization," *Engineering Optimization,* vol. 44, no. 2, pp. 175-194, 2012.

[23] N. Hansen and A. Ostermeier, "Completely derandomized self-adaptation in evolution strategies," *Evolutionary computation,* vol. 9, no. 2, pp. 159-195, 2001.

[24] N. Hansen, S. Finck, R. Ros and A. Auger, "Real-parameter black-box optimization benchmarking 2009: Noisy functions definitions," 2009. [Online].

[25] N. Hansen, "Benchmarking a BI-population CMA-ES on the BBOB-2009 noisy testbed," in *Proceedings of the 11th Annual Conference Companion on Genetic and Evolutionary Computation Conference: Late Breaking Papers*, 2009.